Article

Externally Applied Electromagnetic Fields and Hyperthermia Irreversibly Damage Cancer Cells

Elena Obrador , Ali Jihad-Jebbar , Rosario Salvador-Palmer , Rafael López-Blanch , María Oriol-Caballo , María Paz Moreno-Murciano , Enrique Navarro , Rosa Cibrian , José M. Estrela *

Posted Date: 8 May 2023

doi: 10.20944/preprints202305.0485.v1

Keywords: Non-ionizing radiations; Electromagnetic fields; Hyperthermia; Cancer therapy; Cancer cell death

Article

Externally Applied Electromagnetic Fields and Hyperthermia Irreversibly Damage Cancer Cells

Elena Obrador [1,2], Ali Jihad-Jebbar [1], Rosario Salvador-Palmer [1], Rafael López-Blanch [1,2], María Oriol-Caballo [1,2], María Paz Moreno-Murciano [2], Enrique Navarro [2,3,4], Rosa Cibrian [1,2] and José M. Estrela [1,2,5,*]

[1] Department of Physiology, Faculty of Medicine & Odontology, University of Valencia, 46010 Valencia, Spain; elena.obrador@uv.es (E.O.), ajijeb@alumni.uv.es (A.J.J.) rosario.salvador@uv.es (R.S.P.), loblanch@alumni.uv.es (R.L.B.), maria.oriolc@gmail.com (M.O.C.), rosa.m.cibrian@uv.es (R.C.)
[2] Scientia BioTech, 46002 Valencia, Spain; paz.moreno72@gmail.com (P.M.M.), enrique.navarro@uv.es (E.N.),
[3] Department of Computer Sciences, Higher Technical School of Engineering, 46100 Burjassot, Spain;
[4] IRTIC Institute, University of Valencia, 46980 Paterna, Spain
[5] Department of Physiology, Faculty of Pharmacy, University of Valencia, 46100 Burjassot, Spain
* Correspondence: jose.m.estrela@uv.es

Simple Summary: Moderate loco-regional hyperthermia (40-45°C) is a therapeutic modality that can improve the effects of chemotherapy and radiotherapy and, in addition, improve our immune response against cancer. However, the effects of these combinations on many different cancers are modest. The use of much higher temperatures (> 60°C, thermal ablation), can cause severe damage to healthy tissues. In fact, our results show that cancer cells show an extraordinary resistance to moderate hyperthermia. However, we found that the combination of hyperthermia (not higher than 52°C) with low strength electromagnetic fields acts synergistically causing irreversible damages to different cancer cells. An association of externally applied energies that can be combined with chemotherapy and/or targeted therapies to achieve a complete cancer eradication. *In vivo*, the energy causing focal hyperthermia can be distributed in multiple beams that can be concentrated in the tumor, thus avoiding damaging the healthy tissues that it passes through.

Abstract: At present, the applications and efficacy of non-ionizing radiations (NIR) in oncotherapy are limited. In terms of potential combinations, the use of biocompatible magnetic nanoparticles as heat mediators has been extensively investigated. Nevertheless, the development of more efficient heat nanomediators that may exhibit high specific absorption rates still is an unsolved problem. Our aim was to investigate if externally applied magnetic fields and a heat-inducing NIR affect tumor cell viability. To this end, under *in vitro* conditions, different human cancer cells (A2058 melanoma, AsPC1 pancreas carcinoma, MDA-MB-231 breast carcinoma) were treated with the combination of electromagnetic fields (EMFs, using solenoids) and hyperthermia (HT, using a thermostated bath). The effect of NIR was also studied in combination with standard chemotherapy and targeted therapy. An experimental device combining EMFs and high intensity focused ultrasounds (HIFU)-induced HT was tested *in vivo*. EMFs (25 μT, 4h) or HT (52°C, 40 min) showed a limited effect on cancer cell viability *in vitro*. However, their combination decreased viability to approx. 16%, 50%, and 21% of controls values in A2058, AsPC1, and MDA-MB-231 cells, respectively. Increased lysosomal permeability, release of cathepsins into the cytosol and mitochondria-dependent activation of cell death are the underlying mechanisms. Cancer cells could be completely eliminated combining EMFs, HT and standard chemotherapy or EMFs, HT and anti-Hsp70-targeted therapy. As a proof of concept, *in vivo* experiments performed in AsPC1 xenografts showed that combination of EMFs, HIFU-induced HT, standard chemotherapy and a lysosomal permeabilizer induces a complete cancer regression.

Keywords: Non-ionizing radiations; electromagnetic fields; hyperthermia; cancer therapy; cancer cell death

1. Introduction

 doi:10.20944/preprints202305.0485.v1

The biological effects of non-ionizing electromagnetic fields (EMFs) have been extensively investigated for decades [1]. Based on the guidelines of the International Commission on non-Ionizing Radiation Protection, "Radiofrequency Electromagnetic Fields" (RF EMFs) is the term used to describe the part of the electromagnetic spectrum comprising the frequency range from 100 kHz to 300 GHz (https://www.icnirp.org). Electric fields result from differences in voltage, whereas magnetic fields result from the flow of electric current. Tumor-treating fields (TTFs) are a type of oncotherapy that uses alternating electric fields of intermediate frequency (~100-500 kHz) and low intensity (1-3 V/cm) to disrupt cell division and promote inhibition of cancer growth [2]. The use of this range of intermediate frequency is based on evidences showing that low-frequency electric fields (<1 kHz) progressively disrupt cell membrane polarization, whereas high-frequency fields (>1000 kHz) cause heating-induced damages due to the vibration of the charged/polar cell molecules [3,4]. The established technique for the application of the TTFs requires the placement of electrodes on the body surface around the focus of tumor growth, so that a potential difference can be generated across the growing cancer [5] (https://www.novocure.com). Charged molecules, if subjected to an electric or an EMF, are affected by the direction and intensity of the energy flow. However, there are key differences in the way electric and magnetic fields interact with charged molecules, i.e. (but not limited to) a) the electric field lines are in the direction of the voltage gradient and do not form a loop, whereas the magnetic field lines are around the currents forming a closed loop; b) the electric field is inversely proportional to the voltage gradient, whereas the intensity of the magnetic field depends on the number of field lines produces by the magnet and the current enclosed in its loop; c) the electric field lines are measured in two dimensions, whereas the magnetic field lines are measured in three dimensions (https://www.niehs.nih.gov). At present, potential applications of non-thermal EMFs on cancer therapy have not been implemented yet [6].

Molecular vibration increases as temperature increases, and hyperthermia (HT) can damage and kill cancer cells. However, in practice, HT-based applications in oncotherapy still face strong limitations [7]. Based on the guidelines of the US National Cancer Institute, HT is a type of treatment in which body tissue is heated to as high as 45°C to help damage and kill cancer cells with little or no harm to normal tissue (http://www.cancer.gov). To this end, suggested techniques include probes that generate energy from microwaves, radio waves, lasers, ultrasounds, perfusion of heating fluids, or heating of an entire body in a heated chamber or hot water (http://www.cancer.gov). All these approaches have potential side effects and limited efficacy [8].

Although electromagnetic and heat energies may affect many different cell functions (e.g. [9]), its association is still underdeveloped as a potential oncotherapy. Magnetic nanoparticles-based HT (used as nano-heaters activated by an external magnetic field) has been investigated. However, the development of efficient heat nanomediators with high specific absorption rate value is essential to overcome some key restrictions [i.e. non-specificity, bioavailability and toxicity] [10]. Up to now, these restrictions have precluded nanoparticles-based HT to reach the clinical practice.

In the present report, we demonstrate that low-range EMFs and HT (without the use of nanomediators) irreversibly damage different cancer cells. To this end our experimental setup had to meet two principles: a) the highest magnetic field strength that does not cause a measurable temperature rise in a thermostated environment at 37°C (the internal temperature in mammals), and b) HT should be applied during specific periods of time (which can be achieved *in vivo* and locally by means e.g. of high-intensity focused ultrasounds, HIFU). Our results suggest that this approach may help to overcome the limitations for the use of HT in oncotherapy.

2. Materials and Methods

2.1. Cell culture

Human A2058 (melanoma), AsPC1 (pancreatic adenocarcinoma), and MDA-MB-231 (a hormone-independent breast adenocarcinoma) cells were from the American Type Culture Collection (Manassas, VA). Human AsPC1/Luciferase Stable Cells were obtained from GenTarget Inc. (San Diego CA). Cells were grown in DMEM (Invitrogen, Waltham, MA), pH 7.4, supplemented

Preprints (www.preprints.org) | NOT PEER-REVIEWED | Posted: 8 May 2023 doi:10.20944/preprints202305.0485.v1

with 10% heat-inactivated fetal calf serum (FCS) (Biochrom AG, Berlin, Germany), 100 U/ml penicillin, and 100 µg/ml streptomycin. Cells were plated (20,000 cells/cm^2) and cultured at 37°C in a humidified atmosphere with 5% CO_2. Cells were harvested by incubation for 5 min with 0.05% (w/v) trypsin (Merck, Darmstadt, Germany) in phosphate buffered saline, pH 7.4, containing 0.3 mM EDTA, followed by the addition of 10% FCS to inactivate the trypsin. Cell number and viability were determined using a BioRad (Hercules, CA) TC20 Automated Cell Counter. Cell integrity was also confirmed by measuring leakage of lactate dehydrogenase activity. Cells were allowed to attach for 24 h before any treatment addition.

2.2. Experimental setup for the combined treatment with EMFs and HT in vitro

The source of EMFs was generated with a Promax-GFG-8216 generator (GW Instek, Taipei, Taiwan), adjusted for an output signal of f (frequency)= 100-500 KHz, with an amplitude of 2V. This signal can be visualized with an oscilloscope to check for accuracy of amplitude and f of the sinusoidal signal. The output of the generator was connected with a BCN connector to a coaxial cable of 50 Ω of characteristic impedance, the end of it was soldered to a WE-760308102142 coil from Würth Electronik (Rot am See, Germany). According to the manufacturer's information, the coil has an inductance L = 5.8 µH, and a DC resistance (or ohmic resistance of a conductor) of 0.01 Ω. The calculated skin resistance at e.g. 100 KHz is 0.014 Ω. The coil consists of two superimposed windings, with two parallel copper wires forming a 5-winding flat spiral.

The current can be easily calculated based on the generator output voltage and the coil impedance obtained from the manufacturer, and the magnetic field can be calculated with this current and its geometrical distribution. The WE-760308102142 coil is mathematically modeled as two sets of 10 concentric turns of increasing radius, one set above the other. The outer diameter of the coils was 48.85 mm, and the copper wire had a diameter of 1.5 mm. The magnetic induction B-field (Tesla) along the axis is calculated as follows:

$$B = \frac{\mu_0 I}{2}\left[\sum_{k=1}^{n}\frac{{a_k}^2}{({a_k}^2 + z_1^2)^{3/2}} + \sum_{k=0}^{n}\frac{{a_k}^2}{({a_k}^2 + z_2^2)^{3/2}}\right]$$

Where

$$I = \frac{V}{\sqrt{R^2 + (L\omega - 1/C\omega)^2}}$$

μ_0. Permeability of the free space (vacuum) 1.257 x 10^{-6} (Henry/m).

z_1. Height above the first layer of coil turns (mm).

$z_2 = z_1 + 0.75$ mm.

n = 10. Number of turns of each layer of the coil.

a_k. Radius of each loop (mm).

R. Resistance (Ohm).

V. Output voltage of the generator (Volt).

ω (angular frequency)= $2\pi f$, being f the frequency (Hertz).

L. Inductance of the coil (Henry).

C. Parasitic capacitance of the coil (Farad).

The mathematical equation allows to calculate the magnetic induction B-field (Tesla) along the axis of the coil at 3mm from its surface (approx. 25 µT).

The culture flasks (T25) were placed just above the coil, so that the distance between it and the base of the flask was approx. 3mm. Coil and flask were wrapped in a plastic bag, which in turn was immersed in a thermostated water bath. The temperature of the culture medium was controlled by means of a thermal probe (IKA→ ETS-D5 temperature controller, Merck) placed through the screw cap of the flask. Under these experimental conditions the thermostated water flowing around the culture flask maintained the temperature of the culture medium within the value determined for each experimental condition.

2.3. Flow cytometry and cell death analysis

Preprints (www.preprints.org) | NOT PEER-REVIEWED | Posted: 8 May 2023 doi:10.20944/preprints202305.0485.v1

Cell cycle, viability and death were analyzed with a BD FACSVERSE (Becton Dickinson, Franklin Lakes, NJ). Cell death was measured using propidium iodide and Annexin V-FITC (Thermo Fisher Scientific, Waltham, MA) following the procedure recommended by the manufacturer.

Apoptotic and necrotic cell death were also distinguished by using fluorescence microscopy [11]. To this end, cells were incubated for 3 min with Hoechst 33342 (10 mM; which stains all nuclei) and propidium iodide (10 mM; which stains nuclei of cells with a disrupted plasma membrane), and then analyzed using a Diaphot 300 fluorescence microscope (Nikon, Tokyo, Japan) with excitation at 360 nm. Nuclei of viable, necrotic, and apoptotic cells were detected as blue round nuclei, pink round nuclei, and fragmented blue or pink nuclei, respectively. About 1,500 cells were counted each time. DNA strand breaks in apoptotic cells were assayed by using a direct TUNEL labelling assay (Merck) and fluorescence microscopy following manufacturer's methodology.

2.4. Cytochrome c, apoptosis-inducing factor, and heat-shock proteins

Cancer cells were washed twice with phosphate-buffered saline, and the pellet was suspended in ice-cold homogenization buffer (2 x 10^6 cells per ml of buffer: 20 mM HEPES pH 7.5, 250 mM sucrose, 1 mM $MgCl_2$, 10 mM KCl, 1 mM EDTA, 1 mM EGTA, 1 mM dithiothreitol, 0.1 mM phenylmethylsulfonyl fluoride, and 10 mg leupeptin, aprotinin, and pepstatin A/ml). The cells were homogenized with a Dounce homogenizer. After centrifugation at 2,500 x g for 5 min at 4°C, the supernatants were centrifuged at 100,000 x g for 30 min at 4°C. The resulting supernatant was used as the soluble cytosolic fraction (SCF). Proteins were quantified [12], separated by SDS-PAGE, transferred to nitrocellulose membranes, and probed with anti-cytochrome c (Cyt C) (ab110325, abcam, Cambridge, UK), anti-AIF (sc-55519, Santa Cruz Biotechnology, Santa Cruz, CA), anti-heat-shock protein (Hsp) 70 (ab194360, abcam) and anti-Hsp110 (ab108625, abcam) monoclonal antibodies. Blots were developed using horseradish peroxidase-conjugated secondary antibody and enhanced chemiluminescence (ECL system; GE HealthCare Life Sciences, Malborough, MA). Protein bands were quantitated using a Bio-Rad Gel Doc Go Imaging System.

2.5. Mitochondrial membrane potential

Quantitative determination of the mitochondrial membrane potential (MMP) was performed by the uptake of the radiolabeled lipophilic cation methyl triphenylphosphonium (TPMP), which enables small changes in potential to be determined [13]. Briefly, cancer cells (2 x 10^6) were incubated at 37°C for 60 min in 1 ml DMEM, supplemented as mentioned above but including 1 mM TPMP, 250 nCi [^{3}H]TPMP (Amersham, Bucks, UK), and 1 mM sodium tetraphenylboron. After incubation, the cells were pelleted by centrifugation (1,000 x g for 5 min), 100 ml of the supernatant were removed, the pellet resuspended in 100 ml 10% Triton X-100, and the radioactivity (disintegrations/min) was measured using a Tri-Carb Liquid Scintillation Counter from Perkin-Elmer (Waltham, MA). Non-specific TPMP binding was corrected as previously described [13]. Energization-dependent TPMP uptake was expressed as an accumulation ratio in units of [(TPMP/mg protein)/(TPMP/ml supernatant)] [14].

2.6. Oxygen consumption

O_2 concentration and consumption in isolated cancer cells were measured using an oxygraph of OROBOROS Instruments (Innsbruck, Austria) and as previously described [15].

2.7. H_2O_2 and $O_2^{\cdot-}$

Quantitative measurement of H_2O_2 and $O_2^{\cdot-}$ generation followed previously described methodology [15].

2.8. Cancer cell compartmentation

 doi:10.20944/preprints202305.0485.v1

Cytosolic (cyt) and mitochondrial (mt) compartments were rapidly separated, as previously reported in detail for cancer cells [16], using digitonin and centrifugation through a layer of silicon oil.

2.9. ATP

ATP levels were measured fluorimetrically following standard enzymic methods [17].

2.10. Glutathione

Glutathione (GSH) was determined by LC/MS as previously reported [18]. Cell processing was performed according to published methodology, where rapid N-ethylmaleimide derivatization was used to prevent GSH auto-oxidation [19].

2.11. Caspase 3

This activity was measured by using a highly sensitive colorimetric substrate, N-acetyl-Asp-Glu-Val-Asp p-nitroanilide (Ac-DEVD-pNA) following manufacturer's instructions (CalBiochem, La Jolla, CA). Briefly, cancer cells were lysed in lysis buffer [50 mM HEPES (pH 7.4), 100 mM NaCl, 0.1% (v/v) CHAPS, 1 mM dithiothreitol and 0.1 mM EDTA] on ice for 10 min, then centrifuged at 10,000 x g for 10 min at 4°C. Equal volumes of the supernatants were added to equal volumes of assay buffer [50 mM HEPES (pH 7.4), 100 mM NaCl, 0.1% (v/v) CHAPS, 10 mM dithiothreitol, 0.1 mM EDTA, and 10% glycerol] and incubated at 37°C for 10 min. Then, freshly prepared Ac-DEVD-pNA (200 mM) was added to the mixture and A405 was monitored every 20 min for 3 h at room temperature. Cultures without cell lysates were used as controls. Enzyme activity was calculated, using manufacturer's formulae, as pmol/min.

Z-DEVD-FMK (Z-Asp-Glu-Val-Asp-fluoromethylketone; CalBiochem), dissolved in DMSO and added in a 0.2% volume to give the concentration indicated in the Results section, was used as an irreversible caspase 3 inhibitor.

2.12. Lysosomal membrane integrity

We used LysoTracker™ Deep Red (Thermo Fisher Scientific), a deep red-fluorescent dye for labeling and tracking acidic organelles in live cells. Fluorescence microscopy was run at 577/590 nm (excitation/emission). All the procedure was performed following the manufacturer's recommendat.

2.13. Cathepsin activities

Cancer cell lines were seeded in T25 flasks and, 24 h later, were treated as indicated in the results section. After removal of the medium, extraction buffer containing different concentrations of digitonin (Merck) was used to separate cytosolic and total cathepsins. When necessary, the concentration of digitonin was optimized for different cell types. Cells were incubated with ice-cold lysis buffer (CelLytic™ MT Mammalian Tissue Lysis/Extraction Reagent) containing a protease and phosphatase inhibitors cocktail (Merck) for 15 minutes at 4°C on a rocking platform. Cysteine (Cys) and aspartate (Asp) cathepsin activities were measured using the fluorescent substrates zFR-AFC (AFC= 7-Amino-4-trifluoromethylcoumarin) (excitation at 405 nm; emission at 510 nm) and MCA-GKPILFFRLK(Dnp)-DR-NH2 [MCA= (7-methoxycoumarin-4-yl)acetyl; Dnp= dinitrophenyl] (excitation at 320 nm; emission at 420 nm) (Enzo Biochem, New York, NY), respectively. Pepstatin A (5 mg/ml) and Leupeptin (50 mg/ml) (Merck) were used to inhibit the activity of aspartyl peptidases and serine-cysteine proteases, respectively.

2.14. Gene silencing

Human Hsp70-specific small hairpin RNA (shRNA) was obtained and transfected following the methodology described by Zhu et al. for hepatocellular carcinoma HepG2 cells [20].

2.15. Tumor xenografts

 doi:10.20944/preprints202305.0485.v1

AsPC1 cells, cultured and harvested as explained above, were washed and resuspended in DMEM, and inoculated subcutaneously in the lateral part of the body (5 x 10^6 cells/nu-nu mouse, female, 12 weeks old, Charles River Laboratories). Mice were fed a standard diet (Letica, Rochester Hills, MI). Tumor growth was measured every 2 days using calipers. Tumor volume was calculated in mm^3 based on the following formula, volume = 0.5a x b^2, where a and b are the long and short diameters, respectively. Bioluminiscence detection of cancer cell activity was performed by injecting (i.p.) IVIS brite D-Luciferin Potassium (150 mg/kg, Perkin-Elmer, Waltham, MA) into AsPC1/Luciferase Stable Cells -bearing mice. Bioluminiscence was detected using an IVIS Spectrum *In Vivo* Imaging System (Perkin-Elmer).

2.16. Experimental setup for in vivo treatment

Our experimental setup was based on a technique previously described by Park et al. [21]. Mice were anesthetized with isoflurane, placed and fixed on a methacrylate platform, and their body immersed (up to the neck) in a degassed water bath (24 L, 40 x 30 x 20 cm) thermostated at 37°C. A solenoid (similar to that used *in vitro*, see above) was placed closed to the tumor to ensure that it received approx. 25 μT. The HIFU was composed of two spherical piezoelectric elements with 1.0 MHz resonance frequency, 500 W of acustic potency (rms), and a diameter of 60 mm (Scientia BioTech, Valencia, Spain). The piezoelectric elements were placed to emit 2 ultrasonic beams that impacted the tumor, one vertically to the tumor and the other perpendicular to the previous one. This arrangement was designed in such a way that the energy dissipated was as less damaging as possible to non-cancerous tissues. In the center of one of the piezoelectric elements, an ultrasound scanner was used as a guide to monitor the image of the tumor. This system allows 3D tissue reconstruction for planning, and 2D imaging for monitoring during treatment. The system was adjusted so that the two ultrasonic beams emitted by the piezoelectric elements hit approximately the center of the tumor. During treatment with non-ionizing radiations no noticeable motion was observed in the real-time monitored ultrasound images of the tumor. Mice were treated once per day per three consecutive days. In each session, mice were subjected during 40 min to the combined effect of EMFs and the HIFU-induced HT. The total energy generated by the two HIFU transducers in the tumor was that corresponding to a potency of approx. 60 W/cm^2. To make sure that under our experimental condition, a temperature of approx. 52°C is reached within the tumor, in previous control experiments a thermocouple (TE connectivity, Schaffhausen, Switzerland) was inserted in different AsPC1 tumors *in vivo*. Then the tumors were subjected to HIFU radiation to make sure which potency was necessary to reach the required temperature. The aim of this protocol was to maximize the anticancer effect as much as possible, but taking into account the limitations of the *in vivo* model. Before each session in the bath, mice were pretreated x 12h with EMFs in animal housing cages. These cages were surrounded by an attached network of copper cables that allowed the tumor-bearing mice to constantly receive approx. 25 μT. The aim of this procedure was to try to maximize the effect of the EMFs on the growing tumor. Gemcitabine (50 mg/kg) was administered 1h before each 3-day treatment period (see the Results section).

2.17. Pterostilbene levels

The analysis was performed by liquid chromatography and mass spectrometry (LC-MS/ MS) as previously described [22].

2.18. Evaluation of therapy-induced in vivo toxicity.

This included the following parameters: animal weight, complete blood cell count, and standard blood chemistry.

2.19. Statistical analysis

Data are presented as mean values ± SD for the number of different experiments. Data were analyzed by one- or two-way analysis of variance (ANOVA) or unpaired t tests where appropriate

 doi:10.20944/preprints202305.0485.v1

(SPSS Statistics 29 for Windows; SPSS Inc., Chicago, IL). The homogeneity of the variances was analyzed by the Levene test. The null hypothesis was accepted for all the values of the tests in which the F value was nonsignificant at $p > 0.05$. The data for which the F value was significant was examined by Tukey's test at $p < 0.05$.

3. Results

3.1. EMFs and HT decrease cancer cell viability

As explained in the Introduction and based on the experimental setup (see under Materials and Methods), exposure to EMFs did not associate to an increase in the cell culture temperature above 37°C. On the other hand, the protocol to generate HT under *in vitro* conditions was designed thinking in its potential application *in vivo*. An eventual *in vivo* approach to increase the tumor temperature should be a) rapid and specifically focused in the tumor, and b) in a scale of temperature that should cause limited damage to normal tissues near the tumor. To this end we subjected the cancer cells to a range of temperature from 37°C to a maximum of 52°C. This range of temperature is easy to reach with different methodologies, and (if correctly focused in the tumor) should cause limited side effects in normal peritumoral tissues. As a proof of concept we inoculated subcutaneously AsPC1 cancer cells into nude immunodeficient mice ($n = 5$) [22]. Two weeks after inoculation, the tumor volume reached 75-100 mm^3, and it was heated *in vivo* during 20 or 40 min with an experimental HIFU device bearing a single transducer (Holosonic S.L., Valencia, Spain). We observed that a) the internal temperature of the animal (controlled by a thermal probe placed in the rectum) remained below 38°C; whereas b) the temperature of the tumor (controlled by a probe placed on the peritumoral skin) could be increased up to 52°C in less than 1 min. The spatial shape of the HIFU beam was Gaussian providing enough accuracy in heating the tumor, therefore only the skin surrounding the tumor showed inflammation (grade 2 after 20 min and grade 3 after 40 min of HIFU treatment). Inflammation was scored from 0 to 4 as follows: 0 (none), 1 (apparent increase in polymorphonuclear leukocytes in vessels and migration of these cells into the adjacent tissue in the vicinity of the vessels), 2 (more diffuse, but still relatively sparse inflammation), 3 (intermediate between 2 and 4) and 4 (maximum density of polymorphonuclear leukocytes). Once the HIFU energy was stopped, the tumor temperature returned to 37°C in less than 2 min, a temperature decrease favored by the well-known physiological heat-loss mechanisms. This preliminary *in vivo* experiment confirmed that focused HT (even as high as 52°C) is feasible and may have limited side effects.

As shown in Figure 1A, under *in vitro* conditions, EMFs (100-200 kHz x 4h) very slightly affect the viability of three different cancer cell lines. HT up to 52°C x 40 min caused a significant (although limited) decrease in viability (to approx. 72% in A2058, 77% in AsPC1, and 46% in MDA-MB-231 cells of control values) (Figure 1B). However, as shown in Figure 1C, the combination of EMFs and HT caused a much higher decrease in cell viability (to approx. 16%, 50%, and 21% of controls values in A2058, AsPC1, and MDA-MB-231 cells, respectively) after the 4h-protocol described in the caption of Figure 1. Importantly, in the following 24h-period, tumor cell population did not recover, and viability further decreased to approx. 2.1% (A2058), 3.8% (AsPC1) and 1.6% (MDA-MB-231) of control values (Figure 1C). Thus, indicating that the damage caused by the combination of non-ionizing radiations (NIR) is severe. Nevertheless, this dramatic decrease in cell viability could be misleading since cancer cells, under *in vivo* conditions, may implement mechanisms to resist the effect of NIR, adapt, survive, and grow again. Moreover, *in vivo*, the complex structures surrounding the tumor (stroma, vasculature, and other cells), plus paracrine and systemic factors, may favor their survival. We know that even a small % of a surviving tumor can follow, *a posteriori*, an explosive growth pattern. Thus, it is key to consider that the combination of EMFs and HT may not be enough and should be combined with other oncotherapies.

As shown in Figure 2A, treatment with EMFs and HT (4-h protocol, as in Figure 1C) did not cause significant changes in the cell cycle distribution of the cancer cells studied. However, it is remarkable that EMFs and HT-induced loss of cell viability is mainly associated with a massive apoptosis (Figure 2B). The effect of EMFs or HT, assayed separately, did not change this trend, e.g.

Preprints (www.preprints.org) | NOT PEER-REVIEWED | Posted: 8 May 2023 doi:10.20944/preprints202305.0485.v1

in the case of A2058 cells, the small decrease in cell viability induced by EMFs or HT (Figure 1B) is also associated with apoptosis (approx. a 71 ± 7 % of non-viable cells in the case of EMFs and 87 ± 6 % in the case of HT were identified as apoptotic, n = 5 in both cases). Inverted microscope images showed that EMFs + HT treatment causes drastic changes in the shape of cultured cancer cells (Figure 3A). Importantly, cells treated with EMFs and HT did not recover in the following 24 h (Figure 3A). Thus suggesting that a) the damage caused to the cancer cells is not reversible, and b) the few remaining cells could possibly be in a position of particular weakness against the cytotoxic effect of chemotherapeutic drugs. Cell death analysis (Figure 3B) and the increase in the cytosolic detection of apoptosis-inducing factor and cytochrome C (Figure 3C) further confirmed the EMFs and HT-induced activation of apoptotic cell death.

3.2. EMFs and HT increase ROS generation and the release of death signals from mitochondria

The induction of cell death by EMFs and HT was further analyzed. We focused our experiments on the combination of EMFs and HT because of their superior effect of cancer cell viability. As shown in Table 1, treatment with EMFs and HT increases O_2 consumption and generation of reactive oxygen species (ROS) in the cancer cells. These effects associate to a decrease in mitochondrial membrane potential (MMP), glutathione (mtGSH) and ATP (mtATP) [all consequence of the damage caused by the increase in ROS [23]]; and also to an increase in the cytosolic caspase 3 activity (Table 1), AIF and cytochrome C (Figure 3B) [(key executioners of apoptosis [24]]. All together, these experimental facts prove that EMFs and HT activate the molecular mechanisms of mitochondria-dependent apoptotic death. It is known that inhibition of cellular energy production, generation of ROS, imbalance of cellular Ca^{2+} homeostasis or extracellular cell death signals, are all stimuli capable to induce either apoptosis or necrosis. The relative rate of these two processes (protease and endonuclease activation versus bioenergetic catastrophe) determines whether a cell will undergo primary necrosis or apoptosis [24], a fact that usually resembles the heterogeneity of a growing cancer cell population. Despite this, EMFs and HT mainly cause cancer cell death by apoptosis, whereas only a small % corresponds to necrosis (Figure 2B). From here, it remains to be elucidated whether the activation of cell death is a direct consequence of the action of NIR on mitochondria or secondary to other mechanism(s).

3.3. EMFs and HT increase lysosomal permeability

The cellular heat shock (HS) response involves the heat-shock proteins (HSP). The Hsp70 is the main HSP system, provides thermotolerance and has a central role in translation, post-translation, prevention of aggregates and refolding of aggregated proteins [25]. Hsp110, a cofactor of Hsp70, can provide further tolerance upon cell exposure to extreme temperatures [26]. In the cancer cells, Hsp70 could be key, since it is overexpressed in different cancers and also plays an anti-apoptotic role favouring cancer cell survival (e.g. [27]). As shown in Figure 4A, Hsp70 levels are not significantly affected upon exposure to EMFs and HT (4-h protocol, as in Figure 1C), and only 24h after exposure with we observed in MDA-MB-231 cells a decrease of approx. 36% as compared to controls. However, Hsp110 practically disappears after exposure to EMFs and HT, and its levels do not recover in the following 24-h period (Figure 4A). These results show, in different cancer cells, that Hsp70 levels remain at (or close to) control values despite exposure to EMFs and HT.

Nylandsted et al. [28] reported that Hsp70 is found in the lysosomes of the cancer cells but rarely in those of normal cells, thus facilitating cancer cell survival by keeping lysosomal integrity. HSPs normally bind to lipid membranes and facilitate plasma membrane stabilization during stress conditions [29]. Lysosomal membrane permeabilization (LMP) associates with the release to the cytosol of cysteine and aspartate cathepsins [30], which are known inducers of apoptotic cell death [31].

As shown in Figure 4B, treatment with EMFs and HT (4-h protocol, as in Figure 1C) causes an increase in cytosolic cathepsin activities (see also Figure 4C showing lysosomal content diffusing into the cytosol), thus suggesting that this increase could be the underlying mechanism activating the mitochondria-dependent apoptotic cells death (Figure 2B). To prove this hypothesis, we silenced

 doi:10.20944/preprints202305.0485.v1

Hsp70 expression in AsPC1 cells before subjecting them to the effect of EMFs and HT. We used these cells as a proof of concept because of their relative resistance to EMFs+HT in the short-term (4h) (Figure 1C). EMFs and HT (4-h protocol, as in Figure 1C), caused a decrease in wild-type AsPC1 cell viability to approx. 47 % of control values (necrotic cells, based on microscopic analysis, were < 4% of non-viable cells). The same EMFS and HT-induced stress in Hsp70-knockout (shRNA-dependent) AsPC1 cells, drastically decreased viability to approx. 5 % of control values (% of apoptotic and necrotic cells, based on microscopic analysis, was of approx. 27 and 73% of non-viable cells, respectively) ($p < 0.01$ comparing Hsp70-knockout versus wild-type AsPC1 cells, $n = 5$). The Additional file 1: Figure S1 shows that, in AsPC1 cells treated with EMFs and HT, the activity of cytosolic cathepsins further increases in the Hsp70-knockout cell subset. The higher % of necrotic cells in Hsp70-knockout AsPC1 cells is not surprising, since massive LMP typically results in subapoptotic or necrotic cell death [30]. Taken together, these data suggest a direct relationship among EMFs and HT-induced LMP, Hsp70, cathepsins, and the activation of the mitochondria-dependent cell death.

3.4. Strategies to complement the anti-cancer effect of EMFs and HT and facilitate the complete elimination of cancer cells

The main goal of any anti-cancer strategy is to achieve the complete elimination of all growing cancer cells. As shown in Figure 1C, in our experimental conditions, exposure to EMFs and HT does not kill all cancer cells. In this, the marked resistance of malignant cells to a temperature as high as 52°C is striking. Nevertheless, as explained above, the extremely low cell viability found 24 h after EMFs and HT treatment, may well be misleading. Thus, in order to make our strategy as efficacious as possible, we investigated first the combination of EMFs and HT with standard chemotherapy currently in use against the types of cancers assayed [32–34]. As shown in Figure 5, the combination of EMFs, HT (4-h protocol as in Figure 1C) and paclitaxel (PAC, in A2058 and MDA-MB-231 cells) or gemcitabine (GEM, in AsPC1 cells) drastically decreased cancer cell viability to approx. 2.6 (A2058), 5.3 (AsPC1) and 1.7 (MDA-MB-231) % of control values. Cell viability was measured again 24 h after exposure to the combination of EMFs+HT+chemotherapy and no viable cell could be found (Figure 5). In this last 24-h period the culture medium was renewed to eliminate the presence of PAC or GEM. Both drugs were incubated at concentrations (1 μM PAC, 25 μM GEM) that reflect bioavailable concentrations measured after their *in vivo* administration and during the time period used in our *in vitro* assays.

PAC is administered at doses of 100-250 mg/m^2 IV (24-h infusion) (http://www.cancer.org). Taking the lowest dose of 100 mg/m^2, and approx. 1.8 m^2/70 Kg in humans, that dose means approx. 2.6 mg/Kg x 24h or 0.107 mg/Kg x h (0.428 mg/Kg x 4h). The water content in the human body is of approx. 0.7 L/Kg body weight. Therefore, a patient will receive approx. 0.612 mg of PAC/L of body water x 4h. Since 854 μg of PAC/L are equivalent to 1 μM (just slightly above the concentration expected using the dose of 100 mg/m^2, we used 1 μM PAC in our experiments. In fact, plasma levels of unbound PAC are close to 1 μM during a period of 4-5 h after an IV dose of 135 mg/m^2 [35].

GEM is usually administered at 1000 mg/m^2 IV infusion over 30 min once weekly x 7 weeks (http://www.cancer.org). That means 25.7 mg/Kg x 30 min or 36.7 mg of GEM/L of body water x 30 min. However, although 263 μg of GEM/L are equivalent to approx. 139 μM, mean GEM plasma concentrations range around 32 μM 30 min after a dose of 1000 mg/m^2, 8 μM at 60 min, and undetectable levels at 120 min [36]. Based on this pharmacokinetics, we calculated a concentration of 25 μM to be added to the culture medium 30 min before finishing the 4h-period (as in Figure 1C).

Based on the EMFs and HT-induced LMP effect (see above), alternatively, we also investigated if molecules capable of increasing the LMP could improve the anti-cancer effect of EMFs and HT. To this aim, we assayed first a natural polyphenol, pterostilbene (PT), which has demonstrated LMP properties as well as other anti-cancer effects [37]. As shown in Figure 6, PT (20 μM x 4h) alone very slightly decreased the number of viable cancer cells as compared to control values. The concentration of this polyphenol was selected based on pharmacokinetic criteria [38]. PT can be administered *in vivo* in the form of disodium salt of PT phosphate (LGC Standards, Middlesex, UK) to ensure that the

 doi:10.20944/preprints202305.0485.v1

selected concentration of PT can reach the tumor without systemic side effects during a period equivalent to that used under *in vitro* conditions (Estrela JM, unpublished observations). When EMFs and HT (as in Figure 1C) were combined with PT, the number of viable cancer cells decreased to approx. 7.5 (A2058), 32.7 (AsPC1) and 6.7 (MDA-MB-231) % of control values (Figure 6).

In addition, we assayed a targeted anti-Hsp70 therapy using apoptozole (Az, N-(4-carboxamidobenzyl)-2-(3,5-bis-trifluoromethyl)-4,5-bis-(4-methoxyphenyl)-imidazole, Merck). Az is a small molecule that inhibits the ATPase activity of Hsp70 by binding to

its ATPase domain without affecting other Hsp, and induces apoptotic cancer cell death via caspase activation [39]. The IC50 values of Az were 4.5 ± 0.3, 5.0 ± 0.5 and 4.0 ± 0.2 μM for A2058, AsPC1, and MDA-MB-231 cells, respectively (n = 5 in all cases). As shown in Figure 6, Az alone decreased the number of viable cancer cells to approx. 74 (A2058), 72 (AsPC1) and 60 (MDA-MB-231) % of control values (Figure 6).

When EMFs and HT (as in Figure 1C) were combined with Az, the number of viable cancer cells decreased to 0 (A2058), 7.5 (AsPC1) and 0 (MDA-MB-231) % of control values (Figure 6).

3.5. The combination of EMFs, HT, standard chemotherapy and pterostilbene induces a complete regression of human pancreatic cancer xenografts

As a proof of concept of our therapeutic strategy, we investigated if combination of EMFs and HIFU-induced HT could improve the effect of standard chemotherapy on a human pancreas carcinoma growing in mice. AsPC1 xenografts were treated with gemcitabine, EMFs and HIFU-induced HT, or the triple combination. As shown in Figure 7, gemcitabine, administered at a MTD [40] slightly affected cancer growth (approx. 22% inhibition as compared to controls 35 days after inoculation). The effect of treatment with EMFs and HIFU decreased cancer volume to approx. 14% of controls; whereas the combination of EMFs + HIFU + gemcitabine decreased cancer volume to approx. 3-4% of controls 35 days after inoculation. Importantly, in our experimental conditions, no additional side effects were observed when EMFs and HT were added to the chemotherapy. These results demonstrate the potential efficacy of our strategy. The drastic reduction of pancreatic cancer growth (Figure 7A) may facilitate its elimination by surgery or by treating the tumor-bearing animal/patient with an additional targeted therapy (as suggested above). Based on the data reported in Figure 6, we added PT to the combination of EMFs+HT+gemcitabine. A disodium salt of PT phosphate was administered i.p. (as indicated in the caption of Figure 7). The concentration of PT in the growing tumor was 118 ± 27 μM 30 min after its administration, 59 ± 12 μM (n = 7) at 60 min, and 14 ± 4 μM (n = 7) at 120 min (n = 7 in all cases). As shown in Figure 7B, a complete tumor regression was achieved using the combination of EMFs+HT+gemcitabine+PT, and no tumor cell activity was detected using AsPC1 cells transfected with luciferase (Figure 7C). Mice treated with EMFs+HT+gemcitabine+PT (Figure 7C) were followed up, but tumor growth activity (assayed once a week with the luciferine-luciferase assay) did not recover even 2 months after the completion of the treatment. Two months after treatment all mice followed health evaluation based on the NIH standard methodology (i.e. animal weight, and complete blood cell count and chemistry) (www.nih.gov). Results were similar in control untreated mice and tumor-bearing mice 2 months after the treatment to eradicate the growing cancer (Additional file 2: Table S1). Moreover, data comparing untreated tumor-bearing mice and treated tumor-bearing mice (at day 25, one day after treatment, see Table S1 and Fig. 7A) were not significantly different (results not shown). Which means that changes in weight, hematology and clinical chemistry (Table S1) associate to the growth of the tumor and are not a consequence of the treatment. As a whole, our data indicate that the therapy is safe and does not compromise key parameters linked to the health status in mammals.

3.6. Figures, Tables and Schemes

Preprints (www.preprints.org) | NOT PEER-REVIEWED | Posted: 8 May 2023 doi:10.20944/preprints202305.0485.v1

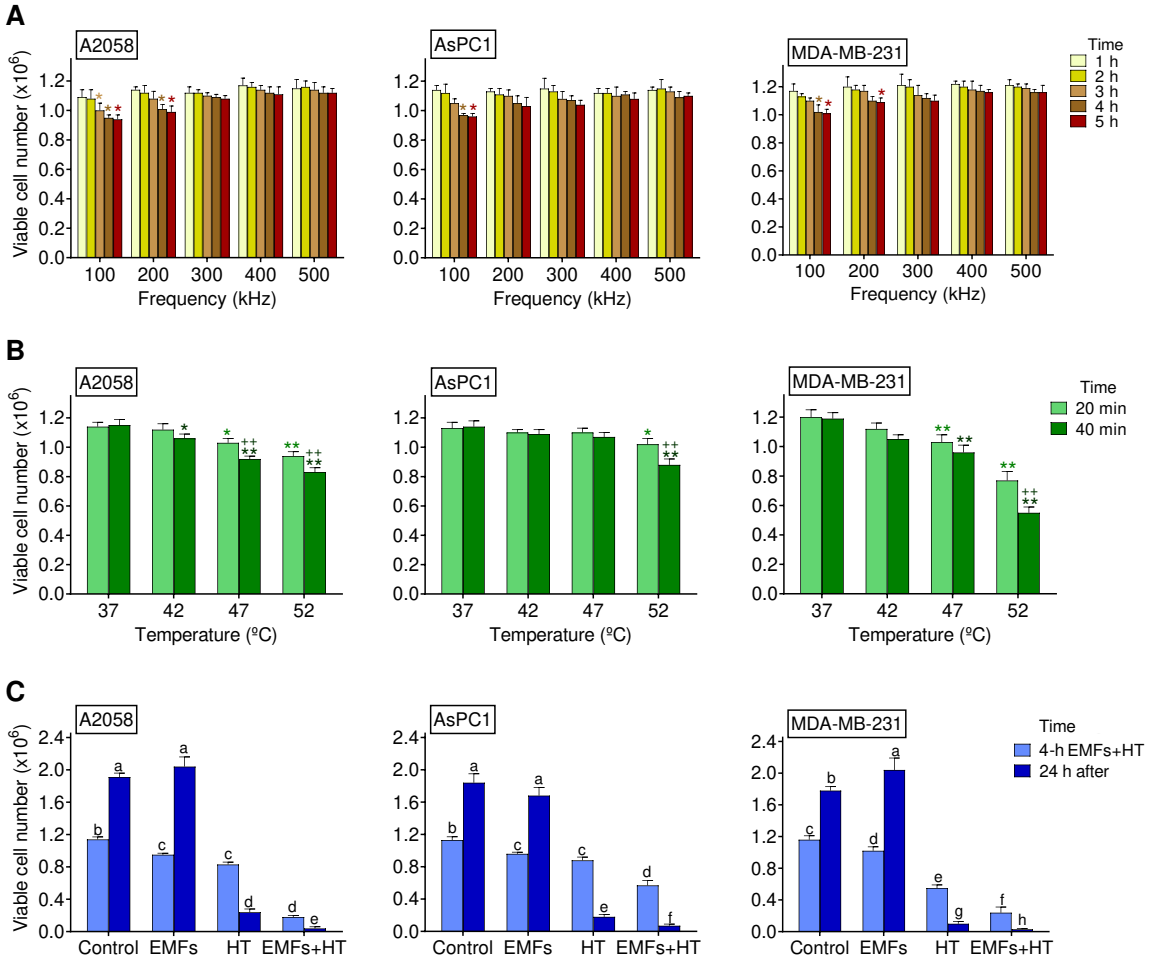

Figure 1. Effect of EMFs and HT on cancer cell viability. (**A**) Effect of EMFs. Cancer cells were seeded and 24 h later exposed to EMFs (100-500 kHz x 1-5 h). Control values (0 kHz) were 1.14 ± 0.03 A2058 1.13 ± 0.04 AsPC1 and 1.20 ± 0.05 MDA-MB-231 (x 10^6) viable cells (n = 5 in all cases). *p < 0.05 comparing all conditions versus controls (0 kHz) (n = 5 t test). (**B**) Effect of HT. Cancer cells were seeded and 24 h later exposed to HT (42-52°C x 20-40 min). *p < 0.05 **p < 0.01 comparing all conditions versus controls (37°C) $^{++}$p < 0.01 comparing 40 min versus 20 min (n = 5 t test). (**C**) Effect of EMFS and HT. Cancer cells were seeded and 24 h later exposed to EMFs (100 kHz x 4h) and HT (52°C x 40 min from min 120 to min 160 of the 4h-period where cells were constantly exposed to the EMFs). Then surviving cells were cultured for 24 additional hours without further exposure to EMFs and HT. A two-ways analysis of variance (ANOVA) was used to make comparisons among the different groups after 4 h of treatment with EMFs+HT and 24 h after. Different letters indicate differences p < 0.05 (n = 5).

Preprints (www.preprints.org) | NOT PEER-REVIEWED | Posted: 8 May 2023 doi:10.20944/preprints202305.0485.v1

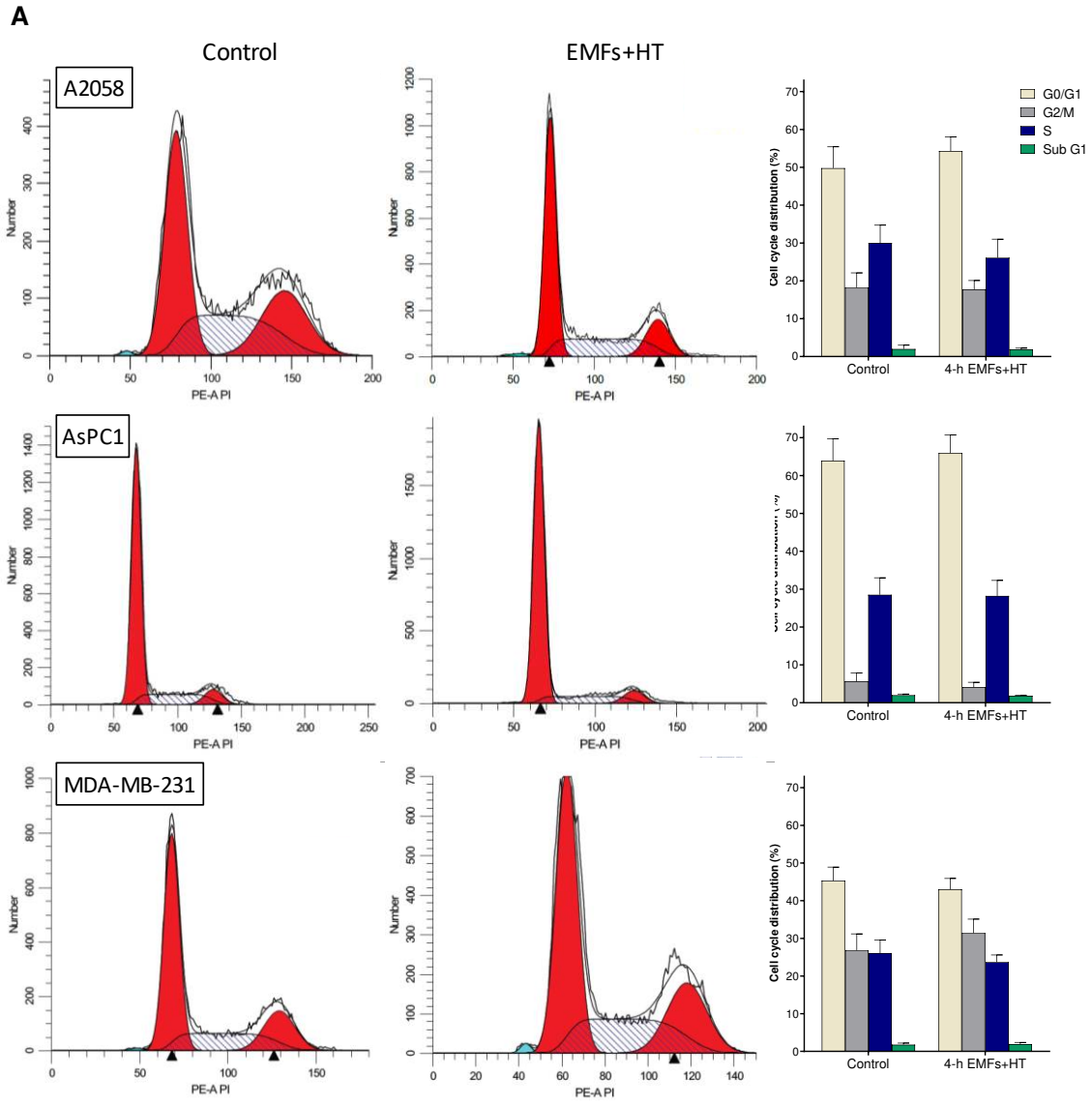

Preprints (www.preprints.org) | NOT PEER-REVIEWED | Posted: 8 May 2023 doi:10.20944/preprints202305.0485.v1

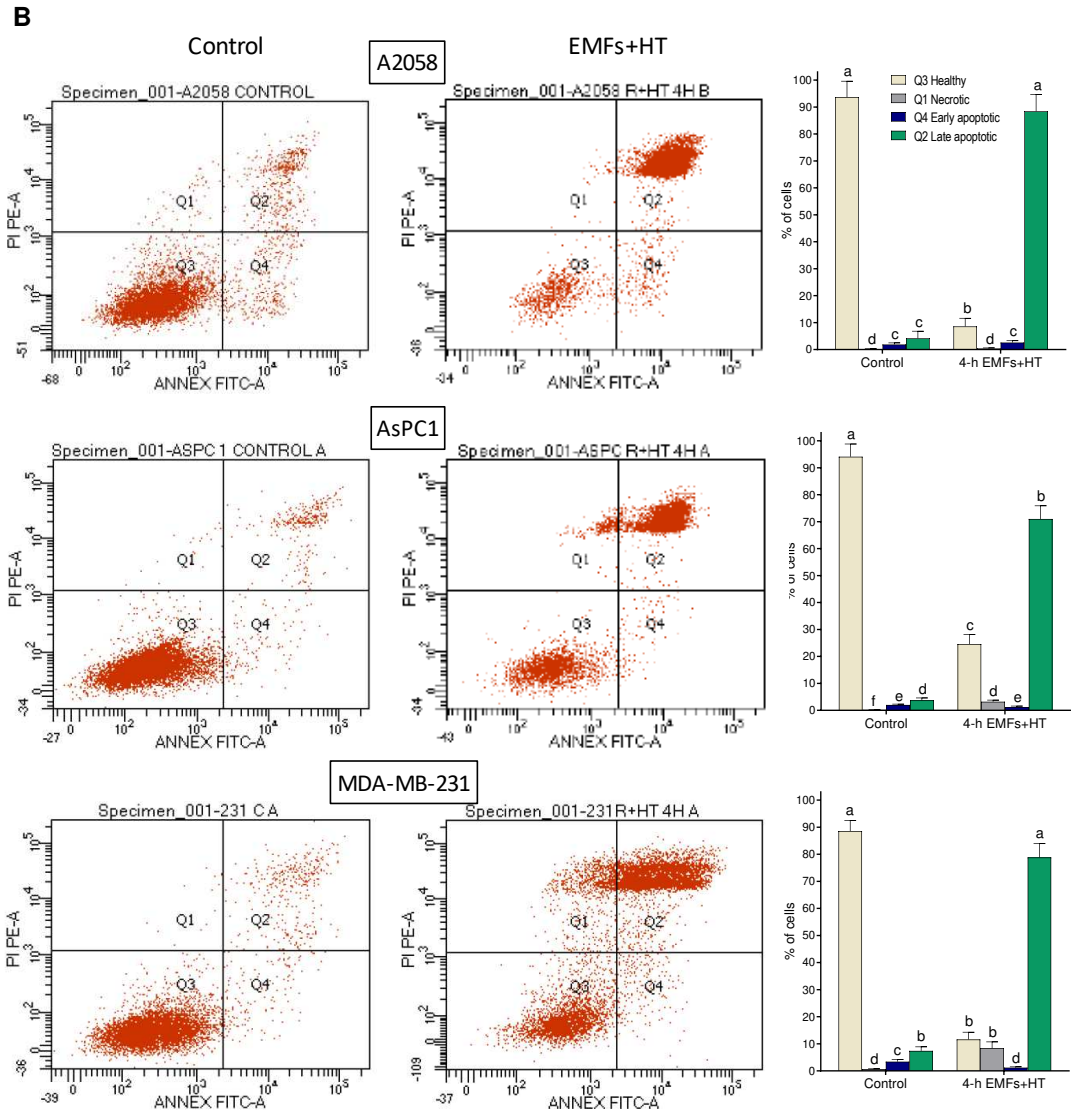

Figure 2. Effect of EMFs and HT on cell cycle distribution and the type of death in cancer cells. (**A**) Flow cytometry analysis of the cell cycle distribution after exposure to EMFs and HT as in Figure 1C (n = 5). No statistically significant differences were found when comparing treatment with EMFs+HT and controls. (**B**) Flow cytometry analysis of EMFs and HT-induced apoptosis and necrosis (treatment as in Figure 1C). A two-ways analysis of variance (ANOVA) was used to make comparisons among controls cells treated with EMFs+HT and the different cell subpopulations in both groups. Different letters indicate differences $p < 0.05$ (n = 5).

Preprints (www.preprints.org) | NOT PEER-REVIEWED | Posted: 8 May 2023 doi:10.20944/preprints202305.0485.v1

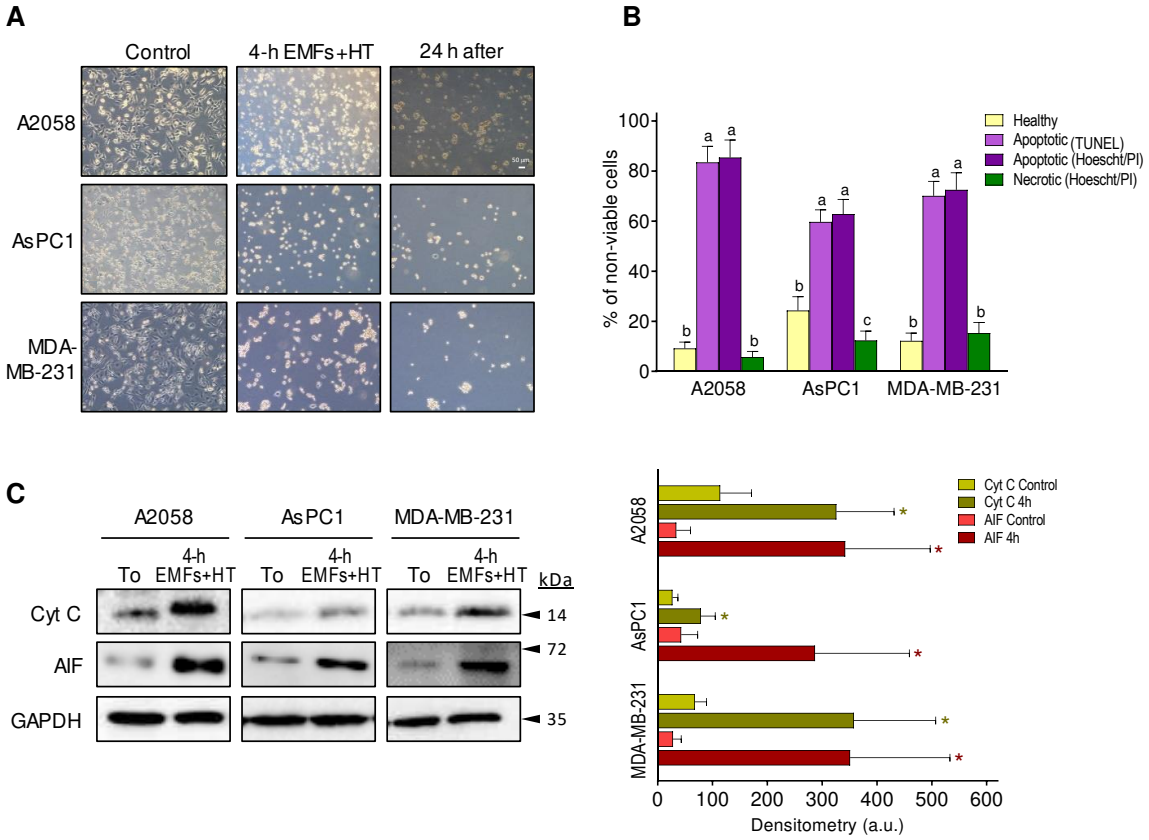

Figure 3. Effect of EMFs and HT on the activation of apoptotic death in cancer cells. (**A**) Inverted microscope images (magnification x 10) of cancer cells treated with EMFs and HT (as in Figure 1C) showing the drastic morphological changes associated with the loss of viability. (**B**) Cell death analysis after the 4-h protocol (Figure 1C) based on Hoechst 33342 and propidium iodide (PI) staining and the TUNEL labeling assay (see under Materials and Methods). Cell viability in control flasks was > 98% in all cases. A one-way analysis of variance (ANOVA) was used to make comparisons among cell subsets. Different letters indicate statistical differences $p < 0.05$ ($n = 5$). (**C**) Western blots for detection of cytochrome C and AIF in the cytosolic fraction (all performed right after the 4-h protocol Figure 1C). Densitometric analysis (a.u. arbitrary units) represents the mean values ± SD for 5 different experiments per cell line [*$p < 0.01$ comparing cells treated with EMFs and HT (4h as in Figure 1C) versus untreated controls t test].

Table 1. Effect of EMFs and HT on ROS generation and the molecular mechanisms of apoptosis.

	A2058		AsPC1		MDA-MB-231	
	-	+ EMFs+HT	-	+ EMFs+HT	-	+ EMFs+HT
O_2 consumption (pmol/10^6 cells x min)	627 ± 79	1067 ± 165**	784 ± 102	1226 ± 188**	551 ± 82	1046 ± 124**
H_2O_2 (nmol/10^6 cells x min)	0.77 ± 0.10	1.56 ± 0.31**	0.94 ± 0.15	1.47 ± 0.27*	0.62 ± 0.13	1.24 ± 0.29**
$O_2^{\cdot-}$ (nmol/10^6 cells x min)	0.33 ± 0.04	0.69 ± 0.12**	0.45 ± 0.07	0.72 ± 0.15**	0.26 ± 0.05	0.48 ± 0.09**
MMP	100 ± 5	42 ± 15**	100 ± 4	56 ± 16**	100 ± 6	35 ± 12**

Preprints (www.preprints.org) | NOT PEER-REVIEWED | Posted: 8 May 2023 doi:10.20944/preprints202305.0485.v1

(TPM accumulation ratio, %)						
mtGSH (nmol/10^6 cells)	4.2 ± 0.9	2.0 ± 0.5**	2.8 ± 0.6	1.3 ± 0.5**	3.5 ± 0.7	1.5 ± 0.5**
mtATP (mM)	1.05 ± 0.10	0.52 ± 0.14**	0.96 ± 0.12	0.41 ± 0.09**	0.92 ± 0.13	0.33 ± 0.08**
Caspase 3 (pmol/10^6 cells x min)	1.87 ± 0.46	3.66 ± 0.39**	1.67 ± 0.35	3.15 ± 0.42**	2.05 ± 0.51	4.14 ± 0.67**

All parameters were measured in cancer cells after exposure to EMFs and HT (4-h protocol as in Figure 1C). *p < 0.05, **p < 0.01 comparing EMFs+HT versus untreated controls (n = 5-6).

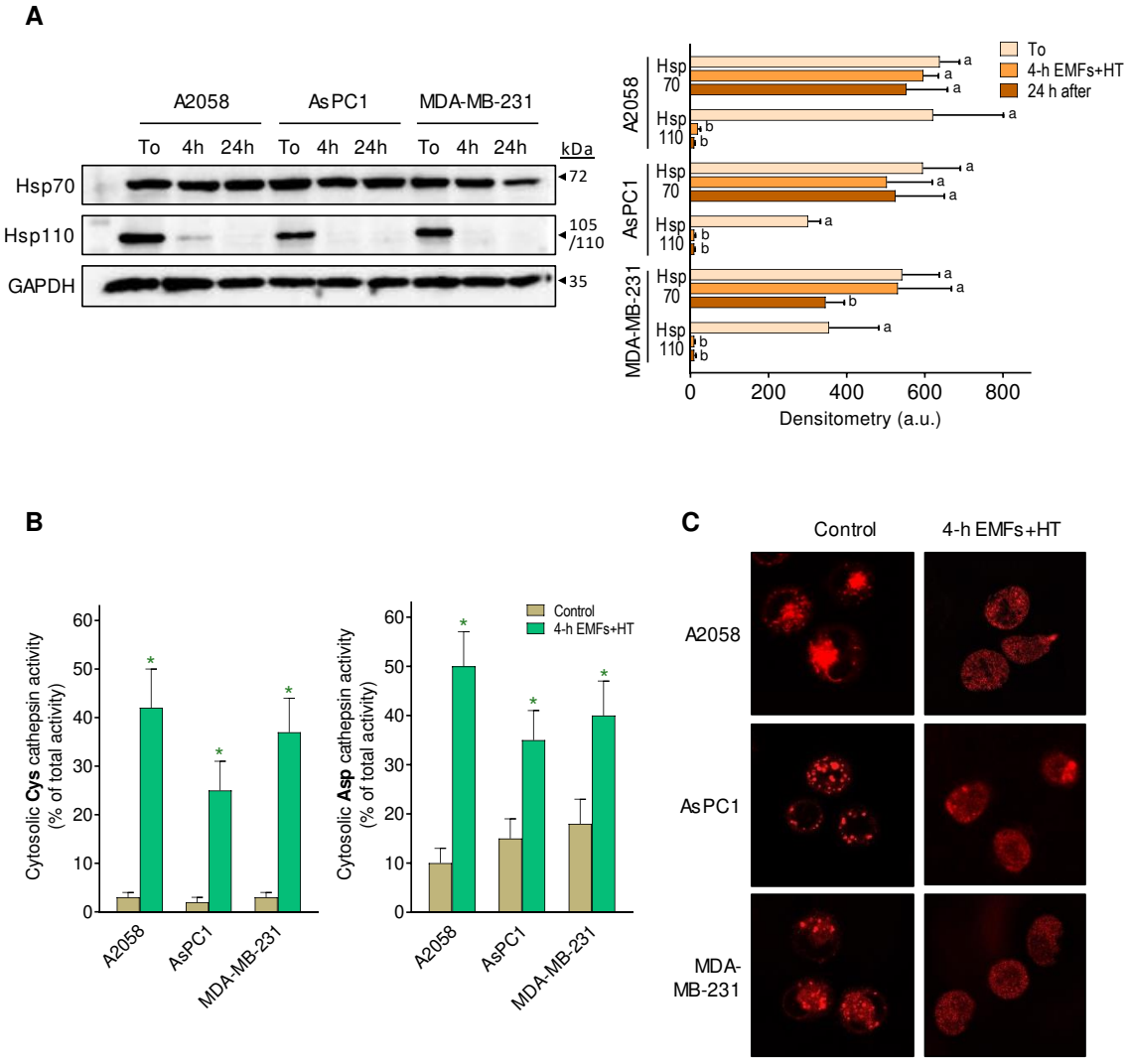

Figure 4. Effect of EMFs and HT on HSP70 and HSP110 and lysosomal permeability. (**A**) Protein levels (western blots) of Hsp70 and Hsp110 were measured in cancer cells after exposure to EMFs and HT (4-h protocol as in Figure 1C) and 24h after exposure (*p < 0.01 comparing EMFs and HT-treated cells versus untreated controls). Densitometric analysis (a.u. arbitrary units) represents the mean values ± SD for 4 different experiments per cell line and time point. A one-way analysis of variance (ANOVA) was used to make comparisons among the different experimental times. Different letters indicate statistical differences p < 0.05. (**B**) Cysteine and aspartate cathepsin activities in the cytosolic fraction were measured after exposure to EMFs and HT (4h-protocol as in Figure 1C) (n = 5 *p < 0.01 comparing

Preprints (www.preprints.org) | NOT PEER-REVIEWED | Posted: 8 May 2023 doi:10.20944/preprints202305.0485.v1

EMFs and HT -treated cells versus untreated controls). (**C**) Lysosome staining (LysoTracker) was performed in the cancer cells (representative images) after the 4-h protocol (as in Figure 1C) showing EMFs and HT-induced diffusion of the lysosomal marker into the cytosol.

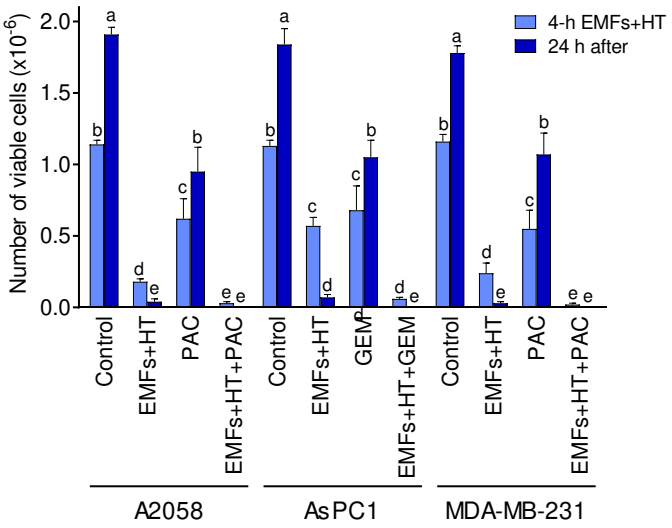

Figure 5. Effect of EMFs HT and chemotherapy on cancer cell viability. Cancer cells were seeded 24 h before starting the treatments. Cells were treated with EMFs and HT (4 h) as in Figure 1C. Paclitaxel (PAC 1 μM) was present in the cultured medium during the 4-h protocol (Figure 1C). Gemcitabine (GEM 25 μM) was present in the cultured medium during the last 30 min of the 4-h protocol. At the end of the 4-h treatment period the culture medium was changed and the cells were kept in culture for 24 additional hours. A two-ways analysis of variance (ANOVA) was used to make comparisons among the different groups after 4 h of treatment with EMFs+HT and 24 h after. Different letters indicate statistical differences $p < 0.05$ ($n = 5$).

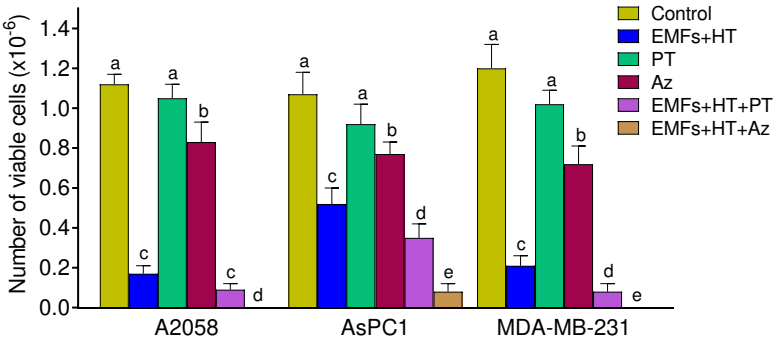

Figure 6. Effect of EMFs HT and a natural lysosomal membrane permeabilizer or a targeted anti-Hsp70 therapy on cancer cells viability. Cells were treated with EMFs and HT as in Figure 1C. Pterostilbene (PT 20 M) or apoptozole (Az 4-5 μM depending on the IC50 values described in the Results section) were added to the cultured medium right before (PT) or 12 h before starting the 4-h protocol (Az) (as in Figure 1C). A one-way analysis of variance (ANOVA) was used to make comparisons among the different experimental groups. Different letters indicate statistical differences $p < 0.05$ ($n = 5$).

Preprints (www.preprints.org) | NOT PEER-REVIEWED | Posted: 8 May 2023 doi:10.20944/preprints202305.0485.v1

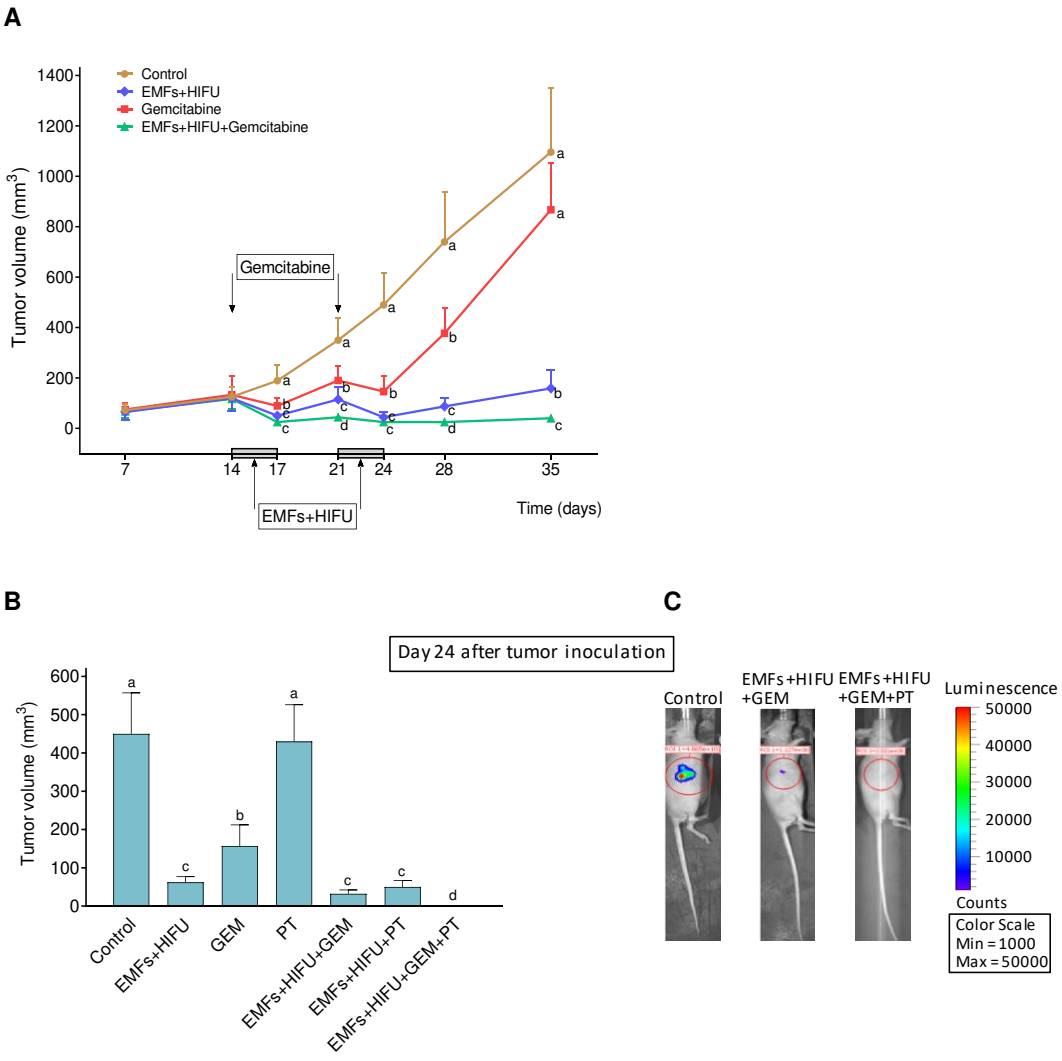

Figure 7. Effect of EMFs + HIFU-induced hyperthermia gemcitabine and/or PT on the growth of AsPC1 pancreas carcinoma. Cancer cells were inoculated subcutaneously on day 0 and mice were treated with EMFs and HIFU as described under Materials and Methods. (**A**) EMFs and HIFU were applied once per day per three consecutive days (Monday to Wednesday) per two consecutive weeks starting on day 14 after tumor inoculation. Gemcitabine (50 mg/kg) was administered twice on days 14 and 21. A one-way analysis of variance (ANOVA) was used to make comparisons among the different experimental groups at each time point. Different letters indicate statistical differences $p < 0.05$ (n = 15 mice per experimental group). (**B**) A disodium salt of PT phosphate (Chromadex Inc. Los Angeles CA) (100 mg of PT/kg) was administered i.p. (one dose 30 min before starting each irradiation session with EMFs and HT). A one-way analysis of variance (ANOVA) was used to make comparisons among the different experimental groups. Different letters indicate statistical differences $p < 0.05$ (n = 12 mice per experimental group). (**C**) Representative images of mice inoculated with AsPC1/Luciferase Stable Cells and treated with EMFs HT and gemcitabine (GEM) or EMFs HT gemcitabine and PT. .

4. Discussion

Do EMFs cause heating of the cells? The mechanism by which the oscillating magnetic field may cause heating of the tissue is by inducing Foucault (or Eddy) currents in the tissue [41]. These currents revolve around the magnetic field lines in the tissue and by the Joule effect could heat the tumor cells. An effect due to the conductivity (σ) of the living tissue. This conductivity provides the path for microscopic Eddy currents which flow in circular paths. The power per unit mass (P) that

 doi:10.20944/preprints202305.0485.v1

heats the cells is given by the following equation: $P = \pi^2.B^2.d^2.f^2/(6.\varrho.D)$. Where B is the magnetic flux density, d is the depth of tissue over which the magnetic field is provided, f is the field frequency, ϱ is the tissue resistivity (inverse to the electrical conductivity) and D is the mass density of the tissue [42].

The conductivity of tumor tissue can be up to five times higher than the conductivity of healthy tissues and has an approximate value of 0.15 Siemens/m at 100-300 kHz [43]. D for biological tissue is variable (between 900-1050 Kg/m^3), but can be approximated by that of the water, 1000 Kg/m^3 [44]. In our experimental setup, the value for P is < 20 pW/Kg, which is very low. The mechanism related to the effect of the EMFs is therefore not due to heating. The synergic effect with hyperthermia could be attributable, at least in part, to an increase of the conductivity associated with an increase in the mobility of the charged molecules.

Methods of heating used for cancer treatment involve a) electromagnetic heating [i.e. in ascending order of frequency and descending penetration depth, capacitive (using metal electrodes and 8-25 MHz) or radiative radiofrequency (using extracorporally placed antennas with operating frequencies ranging from 60MHz to 150 MHz), microwave heating (400-2500 MHz), and infrared (using infrared lamps, frequency > 300 GHz) and laser heating]; b) ultrasounds (acoustic energy at frequencies 0.5–10 MHz); c) hyperthermic perfusion, generally combined with chemotherapy; d) conductive heating, as interstitial implants of metal needles with hot water and palladium–nickel thermoseeds; and e) magnetic nanoparticles, exposed to an external magnetic field (0.1-0.2 MHz) [7]. All these methods have pros and cons. HIFU refer to intensities > $5W/cm^2$, which produce thermal and mechanical effects, generating a localized temperature increase in the tissues. HIFU administration allows a precise treatment of targeted areas, where injury to the surrounding tissue will depend on the temperature reached and the time of exposure. In this regard, since the ultrasonic energy is focused in a specific volume of tissue, it is key to take into account that the temperature will decrease (based on a Gaussian model) as we move away from that specific volume. Therefore, in order to minimize damage to normal tissues but preserving the highest possible efficacy, the combination of EMFs and HIFU may offer the following advantages: a) RF EMFs have not been reported as having any significant toxicity for normal tissues; b) magnetic resonance guided-HIFU (MRgFUS) can target specific volumes of cancers (as small as a few mm of diameter); c) HIFU can be applied using a fast array program (once the target is localized, and the volume and shape of the tumor reconstructed in a computer system, the program can design the sequential application of HIFU at a series of specific points, thus maximizing efficiency; d) to work with EMFs and HIFU allows to limit the rise in temperature to a level that may better preserve the surrounding normal tissues; e) although the number of transducers may need to be increased, depending on the location of the tumor to be treated, a holographic design of the HIFU piezoelectric transducer units (e.g. patent WO2020/084181A1) can reduce their number and, thus, simplify the system; f) the advantage of using multiple transducers is that the energy emitted by each one cannot damage normal tissues, but it can be concentrated in the growing cancer; g) if needed, EMFs and HIFU could be applied several times (e.g. once per day) in order to maximize their efficacy *in vivo*. Based on these technical considerations, the combination of EMFs and HIFU can be easily implemented to transfer our findings to working *in vivo* applications (see Figure 7). Moreover, both, EMFs and HIFU are non-invasive techniques which can be further combined with other anti-cancer therapies (see under Results). In this regard, the present contribution offers some effective options. EMFs and HT can be combined with conventional chemotherapy (Figures 5 and 7). On the other hand, EMFs and HT can also be combined with LMP inducers, as PT or a specific anti-Hsp70-targeted drug (Figure 6). At present, PT has been assayed in clinical trials for different indications, but it has never been administered IV to humans. Interestingly, oral administration of PT cocrystals (as those of PT and picolinic acid, http://www.circescientific.com), which increases PT bioavailability up to 5-10 times compared to that of the natural stilbene alone, can avoid the need of using the IV administration. And, even so, achieving the intratumoral concentration of the polyphenol necessary to increase lysosomal permeability. In favor of the therapeutic use of PT is its potential to decrease Nrf2-dependent antioxidant defenses in cancer cells [22]. On the other hand, trials involving an anti-Hsp70 targeted

 doi:10.20944/preprints202305.0485.v1

therapy are still in their early beginning. Furthermore, recently, some anticancer lysosomotropic drugs (e.g. nortriptyline, siramesine, desipramine) and their nanoformulations have been engineered to specifically accumulate within these organelles. These drugs can enhance LMP or disrupt the activity of resident enzymes and protein complexes, like v-ATPase and mTORC1 [45] (a list of inducers of lysosomal cell death can be found at e.g. [46]). Mechanistically, an increase in cytosolic cathepsin activity triggers the mitochondrial membrane permeabilization through cleavage of Bid, or via activation of phospholipase A2 and the consequent increase in araquidonic acid [47]. Furthermore, cathepsins can directly cause chromatin condensation [48], whereas the cytosol acidification can also lead to L-DNAase II activation and chromatinolysis [49].

Another interesting aspect that deserves further investigation is the possible role of mitochondrial HSP in these mechanisms. ROS generation increases with temperature [50] (Table 1). Thus, it is possible that mitochondrial HSP (Hsp70 in particular), in addition to their roles in protein transport and folding, protect mitochondrial proteins and DNA from thermal and ROS damage.

Initially, there are no reasons that may preclude a multiple combination e.g. EMFs + HT + chemotherapy + a lysosomal permeabilizer, which is also a feasible option in case of finding an unexpected cancer cell resistance *in vivo*. In all this, preclinical studies and clinical trials will be necessary steps. Naturally, there are no strict restrictions in order to combine EMFs and HT with other available (or still being implemented) cancer type-specific therapeutic options, e.g. immunotherapy or signaling-related targeted therapy. It is also important to bear in mind potential counterproductive effects of some lysosomal stabilizers, such as e.g. acetylsalicylic acid or hydrocortisone [51]. These type of drugs should be avoided during cancer treatment with our strategy.

Despite differences in genetic backgrounds and *in vivo* behavior among cancer cells, the combination of EMFS and HT seems to affect them in a similar way (see e.g. Figure 1c) and based on the same mechanism (see e.g. Table 1 and Figure 4). Nevertheless, Hsp70 levels are a clear example of a mechanism of resistance to hyperthermia. Hsp70 inhibits the mitochondrial outer membrane permeabilization, thus reduces caspase activation, and neutralizes the AIF [52]. Moreover, Hsp70 also localizes to lysosomal membranes and can protect LMP induced by different stimuli [53]. Therefore, although eventual mechanisms of resistance to EMFs and HT should be explored in depth, it is encouraging the fact that both energies, if applied at the correct levels and time, appear highly effective both *in vitro* and, as shown in Figure 7, *in vivo*.

5. Conclusions

This work demonstrates that combination EMFs and HT causes an irreversible damage to different cancer cells (i.e. melanoma, pancreatic cancer and breast cancer). The mechanism involves permeabilization of the lysosomes, release of cathepsins to the cytosol, and activation of the mitochondria-dependent cell death. Combination of EMFs and HT with standard chemotherapy, molecules that further promote lysosomal permeabilization, and/or a targeted anti-Hsp70 therapy can completely kill cancer cells. This strategy, supported by *in vitro* and *in vivo* evidences, may complement current oncotherapies and can be applied to different cancers. *In vivo* treated mice followed post-treatment health evaluation (NIH standard methodology), which showed that in our experimental conditions the therapy is safe and *per se* does not compromise mouse physiology.

Supplementary Materials: The following supporting information can be downloaded at the website of this paper posted on Preprints.org. Figure S1. Effect of shRNA-induced downregulation of Hsp70 on the EMFs and HT-induced increase in cytosolic cathepsin activities in AsPC1 cells; Figure S2. Whole blots: (A) Figure 3C, (B) Figure 4A and (C) Figure S1; Table S1. Hematology and clinical chemistry data in AsPC1-bearing mice treated to induced suppression of the growing tumor.

Author Contributions: Conceptualization, J.M.E.; Methodology, all authors; Experimental Work, all authors; Formal Analysis, E.O., R.S.P. and J.M.E.; Original Draft Preparation and Writing, J.M.E.; Review and Editing, R.S.P.; Visualization and Supervision, E.O.; Project Administration, J.M.E.; Funding Acquisition, J.M.E. All authors have read and agreed to the published version of the manuscript.

Funding: This work was supported by a grant (SBT-002) from Scientia BioTech (Valencia, Spain).

Institutional Review Board Statement: All experiments involving animals were in compliance with international laws and policies (EEC Directive 86/609 OJ L 358. 1 December 12 1987 and NIH Guide for the Care and Use of Laboratory Animals NIH Publ. No. 85-23 1985) and approved by the ethics committee in animal experimentation of the University of Valencia Spain (ref. no. A1454405530866).

Informed Consent Statement: Not applicable.

Data Availability Statement: All raw data regarding these studies are available at the Figshare repository (https://doi.org/10.6084/m9.figshare.22220065).

Acknowledgments: We would like to thank the University of Valencia SCIE (Experimental Research Support Service) staff for their technical assistance.

Conflicts of Interest: The authors declare that no competing interests or personal relationships have influenced the work reported in this paper. R. López-Blanch M. Oriol-Caballo and M.P. Moreno-Murciano receive salary support from ScientiaBiotech.

References

1. Saliev, T.; Begimbetova, D.; Masoud, A.-R.; Matkarimov, B. Biological Effects of Non-Ionizing Electromagnetic Fields: Two Sides of a Coin. *Prog. Biophys. Mol. Biol.* **2019**, *141*, 25–36, doi:10.1016/j.pbiomolbio.2018.07.009.
2. Wenger, C.; Miranda, P.C.; Salvador, R.; Thielscher, A.; Bomzon, Z.; Giladi, M.; Mrugala, M.M.; Korshoej, A.R. A Review on Tumor-Treating Fields (TTFields): Clinical Implications Inferred From Computational Modeling. *IEEE Rev. Biomed. Eng.* **2018**, *11*, 195–207, doi:10.1109/RBME.2017.2765282.
3. Chang, F.; Minc, N. Electrochemical Control of Cell and Tissue Polarity. *Annu. Rev. Cell Dev. Biol.* **2014**, *30*, 317–336, doi:10.1146/annurev-cellbio-100913-013357.
4. Krenacs, T.; Meggyeshazi, N.; Forika, G.; Kiss, E.; Hamar, P.; Szekely, T.; Vancsik, T. Modulated Electro-Hyperthermia-Induced Tumor Damage Mechanisms Revealed in Cancer Models. *Int. J. Mol. Sci.* **2020**, *21*, E6270, doi:10.3390/ijms21176270.
5. Arvind, R.; Chandana, S.R.; Borad, M.J.; Pennington, D.; Mody, K.; Babiker, H. Tumor-Treating Fields: A Fourth Modality in Cancer Treatment, New Practice Updates. *Crit. Rev. Oncol. Hematol.* **2021**, *168*, 103535, doi:10.1016/j.critrevonc.2021.103535.
6. Wust, P.; Stein, U.; Ghadjar, P. Non-Thermal Membrane Effects of Electromagnetic Fields and Therapeutic Applications in Oncology. *Int. J. Hyperth. Off. J. Eur. Soc. Hyperthermic Oncol. North Am. Hyperth. Group* **2021**, *38*, 715–731, doi:10.1080/02656736.2021.1914354.
7. Kok, H.P.; Cressman, E.N.K.; Ceelen, W.; Brace, C.L.; Ivkov, R.; Grüll, H.; Ter Haar, G.; Wust, P.; Crezee, J. Heating Technology for Malignant Tumors: A Review. *Int. J. Hyperth. Off. J. Eur. Soc. Hyperthermic Oncol. North Am. Hyperth. Group* **2020**, *37*, 711–741, doi:10.1080/02656736.2020.1779357.
8. Lee, S.-Y.; Fiorentini, G.; Szasz, A.M.; Szigeti, G.; Szasz, A.; Minnaar, C.A. Quo Vadis Oncological Hyperthermia (2020)? *Front. Oncol.* **2020**, *10*, 1690, doi:10.3389/fonc.2020.01690.
9. Silva, P.L.; Savchuk, O.A.; Gallo, J.; García-Hevia, L.; Bañobre-López, M.; Nieder, J.B. Mapping Intracellular Thermal Response of Cancer Cells to Magnetic Hyperthermia Treatment. *Nanoscale* **2020**, *12*, 21647–21656, doi:10.1039/c9nr10370h.
10. Das, P.; Colombo, M.; Prosperi, D. Recent Advances in Magnetic Fluid Hyperthermia for Cancer Therapy. *Colloids Surf. B Biointerfaces* **2019**, *174*, 42–55, doi:10.1016/j.colsurfb.2018.10.051.
11. Shimizu, S.; Eguchi, Y.; Kamiike, W.; Itoh, Y.; Hasegawa, J.; Yamabe, K.; Otsuki, Y.; Matsuda, H.; Tsujimoto, Y. Induction of Apoptosis as Well as Necrosis by Hypoxia and Predominant Prevention of Apoptosis by Bcl-2 and Bcl-XL. *Cancer Res.* **1996**, *56*, 2161–2166.
12. Bradford, M.M. A Rapid and Sensitive Method for the Quantitation of Microgram Quantities of Protein Utilizing the Principle of Protein-Dye Binding. *Anal. Biochem.* **1976**, *72*, 248–254, doi:10.1016/0003-2697(76)90527-3.
13. Scarlett, J.L.; Sheard, P.W.; Hughes, G.; Ledgerwood, E.C.; Ku, H.H.; Murphy, M.P. Changes in Mitochondrial Membrane Potential during Staurosporine-Induced Apoptosis in Jurkat Cells. *FEBS Lett.* **2000**, *475*, 267–272, doi:10.1016/s0014-5793(00)01681-1.

14. James, A.M.; Wei, Y.H.; Pang, C.Y.; Murphy, M.P. Altered Mitochondrial Function in Fibroblasts Containing MELAS or MERRF Mitochondrial DNA Mutations. *Biochem. J.* **1996**, *318 (Pt 2)*, 401–407, doi:10.1042/bj3180401.
15. López-Blanch, R.; Salvador-Palmer, R.; Estrela, J.M.; Obrador, E. An Intercellular Flow of Glutathione Regulated by Interleukin 6 Links Astrocytes and the Liver in the Pathophysiology of Amyotrophic Lateral Sclerosis. *Antioxid. Basel Switz.* **2021**, *10*, 2007, doi:10.3390/antiox10122007.
16. Obrador, E.; Navarro, J.; Mompo, J.; Asensi, M.; Pellicer, J.A.; Estrela, J.M. Glutathione and the Rate of Cellular Proliferation Determine Tumour Cell Sensitivity to Tumour Necrosis Factor in Vivo. *Biochem. J.* **1997**, *325 (Pt 1)*, 183–189, doi:10.1042/bj3250183.
17. Bergmeyer, H.U. *Methods of Enzymatic Analysis*; Verlag Chemie, 1974; ISBN 978-3-527-25370-8.
18. Obrador, E.; Valles, S.L.; Benlloch, M.; Sirerol, J.A.; Pellicer, J.A.; Alcácer, J.; Coronado, J.A.-F.; Estrela, J.M. Glucocorticoid Receptor Knockdown Decreases the Antioxidant Protection of B16 Melanoma Cells: An Endocrine System-Related Mechanism That Compromises Metastatic Cell Resistance to Vascular Endothelium-Induced Tumor Cytotoxicity. *PloS One* **2014**, *9*, e96466, doi:10.1371/journal.pone.0096466.
19. Asensi, M.; Sastre, J.; Pallardo, F.V.; Estrela, J.M.; Viña, J. Determination of Oxidized Glutathione in Blood: High-Performance Liquid Chromatography. *Methods Enzymol.* **1994**, *234*, 367–371, doi:10.1016/0076-6879(94)34106-0.
20. Zhu, Q.; Xu, Y.-M.; Wang, L.-F.; Zhang, Y.; Wang, F.; Zhao, J.; Jia, L.-T.; Zhang, W.-G.; Yang, A.-G. Heat Shock Protein 70 Silencing Enhances Apoptosis Inducing Factor-Mediated Cell Death in Hepatocellular Carcinoma HepG2 Cells. *Cancer Biol. Ther.* **2009**, *8*, 792–798, doi:10.4161/cbt.8.9.8127.
21. Park, E.-J.; Ahn, Y.D.; Lee, J.Y. In Vivo Study of Enhanced Chemotherapy Combined with Ultrasound Image-Guided Focused Ultrasound (USgFUS) Treatment for Pancreatic Cancer in a Xenograft Mouse Model. *Eur. Radiol.* **2018**, *28*, 3710–3718, doi:10.1007/s00330-018-5355-9.
22. Benlloch, M.; Obrador, E.; Valles, S.L.; Rodriguez, M.L.; Sirerol, J.A.; Alcácer, J.; Pellicer, J.A.; Salvador, R.; Cerdá, C.; Sáez, G.T.; et al. Pterostilbene Decreases the Antioxidant Defenses of Aggressive Cancer Cells In Vivo: A Physiological Glucocorticoids- and Nrf2-Dependent Mechanism. *Antioxid. Redox Signal.* **2016**, *24*, 974–990, doi:10.1089/ars.2015.6437.
23. Hayes, J.D.; Dinkova-Kostova, A.T.; Tew, K.D. Oxidative Stress in Cancer. *Cancer Cell* **2020**, *38*, 167–197, doi:10.1016/j.ccell.2020.06.001.
24. Kroemer, G.; Reed, J.C. Mitochondrial Control of Cell Death. *Nat. Med.* **2000**, *6*, 513–519, doi:10.1038/74994.
25. Lepock, J.R. How Do Cells Respond to Their Thermal Environment? *Int. J. Hyperth. Off. J. Eur. Soc. Hyperthermic Oncol. North Am. Hyperth. Group* **2005**, *21*, 681–687, doi:10.1080/02656730500307298.
26. Oh, H.J.; Chen, X.; Subjeck, J.R. Hsp110 Protects Heat-Denatured Proteins and Confers Cellular Thermoresistance. *J. Biol. Chem.* **1997**, *272*, 31636–31640, doi:10.1074/jbc.272.50.31636.
27. Ciocca, D.R.; Calderwood, S.K. Heat Shock Proteins in Cancer: Diagnostic, Prognostic, Predictive, and Treatment Implications. *Cell Stress Chaperones* **2005**, *10*, 86–103, doi:10.1379/csc-99r.1.
28. Nylandsted, J.; Gyrd-Hansen, M.; Danielewicz, A.; Fehrenbacher, N.; Lademann, U.; Høyer-Hansen, M.; Weber, E.; Multhoff, G.; Rohde, M.; Jäättelä, M. Heat Shock Protein 70 Promotes Cell Survival by Inhibiting Lysosomal Membrane Permeabilization. *J. Exp. Med.* **2004**, *200*, 425–435, doi:10.1084/jem.20040531.
29. Calvaresi, V.; Truelsen, L.T.; Larsen, S.B.; Petersen, N.H.T.; Kirkegaard, T.; Rand, K.D. Conformational Dynamics of Free and Membrane-Bound Human Hsp70 in Model Cytosolic and Endo-Lysosomal Environments. *Commun. Biol.* **2021**, *4*, 1369, doi:10.1038/s42003-021-02892-7.
30. Boya, P.; Kroemer, G. Lysosomal Membrane Permeabilization in Cell Death. *Oncogene* **2008**, *27*, 6434–6451, doi:10.1038/onc.2008.310.
31. Stoka, V.; Turk, V.; Turk, B. Lysosomal Cysteine Cathepsins: Signaling Pathways in Apoptosis. *Biol. Chem.* **2007**, *388*, 555–560, doi:10.1515/BC.2007.064.
32. Specenier, P. Efficacy of Nab-Paclitaxel in Treating Metastatic Melanoma. *Expert Opin. Pharmacother.* **2019**, *20*, 495–500, doi:10.1080/14656566.2019.1569628.
33. Abu Samaan, T.M.; Samec, M.; Liskova, A.; Kubatka, P.; Büsselberg, D. Paclitaxel's Mechanistic and Clinical Effects on Breast Cancer. *Biomolecules* **2019**, *9*, E789, doi:10.3390/biom9120789.
34. Sarvepalli, D.; Rashid, M.U.; Rahman, A.U.; Ullah, W.; Hussain, I.; Hasan, B.; Jehanzeb, S.; Khan, A.K.; Jain, A.G.; Khetpal, N.; et al. Gemcitabine: A Review of Chemoresistance in Pancreatic Cancer. *Crit. Rev. Oncog.* **2019**, *24*, 199–212, doi:10.1615/CritRevOncog.2019031641.

35. Brouwer, E.; Verweij, J.; De Bruijn, P.; Loos, W.J.; Pillay, M.; Buijs, D.; Sparreboom, A. Measurement of Fraction Unbound Paclitaxel in Human Plasma. *Drug Metab. Dispos. Biol. Fate Chem.* **2000**, *28*, 1141–1145.
36. Ciccolini, J.; Serdjebi, C.; Peters, G.J.; Giovannetti, E. Pharmacokinetics and Pharmacogenetics of Gemcitabine as a Mainstay in Adult and Pediatric Oncology: An EORTC-PAMM Perspective. *Cancer Chemother. Pharmacol.* **2016**, *78*, 1–12, doi:10.1007/s00280-016-3003-0.
37. Mena, S.; Rodríguez, M.L.; Ponsoda, X.; Estrela, J.M.; Jäättela, M.; Ortega, A.L. Pterostilbene-Induced Tumor Cytotoxicity: A Lysosomal Membrane Permeabilization-Dependent Mechanism. *PloS One* **2012**, *7*, e44524, doi:10.1371/journal.pone.0044524.
38. Priego, S.; Feddi, F.; Ferrer, P.; Mena, S.; Benlloch, M.; Ortega, A.; Carretero, J.; Obrador, E.; Asensi, M.; Estrela, J.M. Natural Polyphenols Facilitate Elimination of HT-29 Colorectal Cancer Xenografts by Chemoradiotherapy: A Bcl-2- and Superoxide Dismutase 2-Dependent Mechanism. *Mol. Cancer Ther.* **2008**, *7*, 3330–3342, doi:10.1158/1535-7163.MCT-08-0363.
39. Ko, S.-K.; Kim, J.; Na, D.C.; Park, S.; Park, S.-H.; Hyun, J.Y.; Baek, K.-H.; Kim, N.D.; Kim, N.-K.; Park, Y.N.; et al. A Small Molecule Inhibitor of ATPase Activity of HSP70 Induces Apoptosis and Has Antitumor Activities. *Chem. Biol.* **2015**, *22*, 391–403, doi:10.1016/j.chembiol.2015.02.004.
40. Awasthi, N.; Zhang, C.; Schwarz, A.M.; Hinz, S.; Wang, C.; Williams, N.S.; Schwarz, M.A.; Schwarz, R.E. Comparative Benefits of Nab-Paclitaxel over Gemcitabine or Polysorbate-Based Docetaxel in Experimental Pancreatic Cancer. *Carcinogenesis* **2013**, *34*, 2361–2369, doi:10.1093/carcin/bgt227.
41. Aguiar, P.M.; Jacquinot, J.-F.; Sakellariou, D. Experimental and Numerical Examination of Eddy (Foucault) Currents in Rotating Micro-Coils: Generation of Heat and Its Impact on Sample Temperature. *J. Magn. Reson. San Diego Calif 1997* **2009**, *200*, 6–14, doi:10.1016/j.jmr.2009.05.010.
42. Peters, M.J.; Stinstra, G.; Hendriks, M. Estimation of the Electrical Conductivity of Human Tissue. *Electromagnetics* **2001**, *21*, 545–557, doi:10.1080/027263401752246199.
43. Miklavčič, D.; Pavšelj, N.; Hart, F.X. Electric Properties of Tissues. In *Wiley Encyclopedia of Biomedical Engineering*; John Wiley & Sons, Ltd, 2006 ISBN 978-0-471-74036-0.
44. Miller, W.H.; Hartmann-Siantar, C.; Fisher, D.; Descalle, M.-A.; Daly, T.; Lehmann, J.; Lewis, M.R.; Hoffman, T.; Smith, J.; Situ, P.D.; et al. Evaluation of Beta-Absorbed Fractions in a Mouse Model for 90Y, 188Re, 166Ho, 149Pm, 64Cu, and 177Lu Radionuclides. *Cancer Biother. Radiopharm.* **2005**, *20*, 436–449, doi:10.1089/cbr.2005.20.436.
45. Allemailem, K.S.; Almatroudi, A.; Alrumaihi, F.; Almatroodi, S.A.; Alkurbi, M.O.; Basfar, G.T.; Rahmani, A.H.; Khan, A.A. Novel Approaches of Dysregulating Lysosome Functions in Cancer Cells by Specific Drugs and Its Nanoformulations: A Smart Approach of Modern Therapeutics. *Int. J. Nanomedicine* **2021**, *16*, 5065–5098, doi:10.2147/IJN.S321343.
46. Domagala, A.; Fidyt, K.; Bobrowicz, M.; Stachura, J.; Szczygiel, K.; Firczuk, M. Typical and Atypical Inducers of Lysosomal Cell Death: A Promising Anticancer Strategy. *Int. J. Mol. Sci.* **2018**, *19*, E2256, doi:10.3390/ijms19082256.
47. Jäättelä, M. Multiple Cell Death Pathways as Regulators of Tumour Initiation and Progression. *Oncogene* **2004**, *23*, 2746–2756, doi:10.1038/sj.onc.1207513.
48. Isahara, K.; Ohsawa, Y.; Kanamori, S.; Shibata, M.; Waguri, S.; Sato, N.; Gotow, T.; Watanabe, T.; Momoi, T.; Urase, K.; et al. Regulation of a Novel Pathway for Cell Death by Lysosomal Aspartic and Cysteine Proteinases. *Neuroscience* **1999**, *91*, 233–249, doi:10.1016/s0306-4522(98)00566-1.
49. Barry, M.A.; Eastman, A. Identification of Deoxyribonuclease II as an Endonuclease Involved in Apoptosis. *Arch. Biochem. Biophys.* **1993**, *300*, 440–450, doi:10.1006/abbi.1993.1060.
50. Slimen, I.B.; Najar, T.; Ghram, A.; Dabbebi, H.; Ben Mrad, M.; Abdrabbah, M. Reactive Oxygen Species, Heat Stress and Oxidative-Induced Mitochondrial Damage. A Review. *Int. J. Hyperth. Off. J. Eur. Soc. Hyperthermic Oncol. North Am. Hyperth. Group* **2014**, *30*, 513–523, doi:10.3109/02656736.2014.971446.
51. Alamo, C.; Ferrándiz, B.; López-Muñoz, F.; Alguacil, L.F. Influence of Butibufen on Enzyme Activity and Lysosomal Stabilization Ex Vivo: A Comparative Study with Hydrocortisone and Acetylsalicylic Acid. *Methods Find. Exp. Clin. Pharmacol.* **1995**, *17*, 303–310.
52. Garrido, C.; Brunet, M.; Didelot, C.; Zermati, Y.; Schmitt, E.; Kroemer, G. Heat Shock Proteins 27 and 70: Anti-Apoptotic Proteins with Tumorigenic Properties. *Cell Cycle Georget. Tex* **2006**, *5*, 2592–2601, doi:10.4161/cc.5.22.3448.
53. Petersen, N.H.T.; Kirkegaard, T.; Olsen, O.D.; Jäättelä, M. Connecting Hsp70, Sphingolipid Metabolism and Lysosomal Stability. *Cell Cycle Georget. Tex* **2010**, *9*, 2305–2309, doi:10.4161/cc.9.12.12052.

 doi:10.20944/preprints202305.0485.v1